Experimental Study on Drag Forces of Non-Spherical Objects in Jets

Chenxi Sun [1,*], Mengxuan Sun [2], Ziming Wang [3] and Longhan Xu [4]

[1] Department of Materials Science and Engineering, Shandong University, Jinan, 250100, China

[2] Nanjing Jinling Middle School Hexi Branch, Nanjing, China

[3] Wuhan Britain-China School, Wuhan, 430050, China

[4] Xi'an Gaoxin No.1 High School, Xi'an, 710075, China

* Corresponding Author Email: 202500150221@mail.sdu.edu.cn

Abstract. Most studies on fluid dynamics only account for spheres in jets. They derive their formula from the Navier-Stokes equation which is only accountable for spheres. However, few can provide a general formula for non-spherical objects since their irregular shape could cause turbulence thus make the accurate measurement difficult. Some of the previous studies investigated the viscous drag on these objects empirically, giving empirical formula using experimental approaches. This study aims to investigate viscous drag on non-spherical objects through stimulating jet conditions using two different experimental set ups, giving experimental results and comment on the empirical formula from previous studies. To begin with, Objects of different masses were tested under fixed wind speeds to measure their stable equilibrium heights, validating theoretical model and formula of drag force in jets with respect to the position inside the jet. Then, another experiment is conducted on non-spherical objects to measure experimental drag force. The experimental result will be compared with the results calculated from the previous empirical formulas, and they will be commented in terms of deviation from the experimental value in terms of accuracy using standard deviation. This research intends to give an insight in to viscous drag on non-spherical bodies using camera-based method and provides a precise measurement and comment onto previous studies.

Keywords: Viscous Drag, Jets, Camera-Based, Spherical, Non-spherical, Empirical Formula.

1. Introduction

Jet is defined as a steam of flow going out of a small orifice [1]. While an object experiences drag force (F_d) in a free fluid condition, the drag force in a free fluid is given by the famous equation: $F_d = \frac{1}{2}\rho C_d A v^2$, where ρ is the density of the fluid, A is characteristic surface area, C_d is the coefficient of drag, and v is the velocity of fluid, the Stoke's law gives the drag force of an isolated sphere objects in a laminar flow. It states that: $F_d = 3\pi\mu d_v v$ where μ is the viscosity of the fluid, and d_v is the diameter of a sphere with the same volume as the object. This report intends to give a model for the drag force for a spherical object at the center of the jet using direct parameter of the jet and the object instead of the general formula. In addition, we will also explore comment on the formula for previous studies on non-spherical using camera based experimental method.

This study investigates the viscous drag of spheres and non-spherical objects in vertical jets, with three primary objectives:

1) To determine a specific theoretical model for viscous drag force on spherical objects in a vertical jet.

2) Explore and extend the model from spherical objects to non-spherical ones by establishing equilibrium for weight and drag and then quantitatively establish an approximate and modified model regarding the object shape, jet velocity, and drag force etc.

Current study on drag in jet mainly focuses on spherical objects under various circumstances such as high Reynolds number case [2], turbulent case [3]. Also, there are some older studies on to the non-spherical ones. K, which is the dynamic shape factor, was introduced to modify the Stoke's law [4].

$$F_d = 3\pi\mu d_v \nu K \tag{1}$$

Studies have been carried out to determine K empirically. Note that the equations below are all for air flow moving in the direction of the axis of symmetry.

For example, Heiss and Coull gave K for cylinders and rectangular prisms [5]:

$$log_{10}(K) = -0.270\frac{\left(\frac{d_v}{d_n}-1\right)}{(\psi)^{0.5}\left(\frac{d_v}{d_n}\right)^{0.345}} + log_{10}\left[\left(\frac{d_v}{d_n}\right)(\psi)^{0.5}\right] \tag{2}$$

Where d_n is the diameter of a sphere whose projected area is the same as the area of the object projected normal to its direction of motion, ψ is the surface area of a sphere with the same volume as the object divided by the surface area of the object.

Bowen and Masliyah gave K for cylinders with flat, hemispherical, and conical ends, for merging spheres, for double-headed cones and cones with hemispherical caps and for spheroids [6]:

$$K = 0.244 + 1.035S - 0.712S^2 + 0.441S^3 \tag{3}$$

Where S is the surface area of the object, divided by surface area of a perimeter-equivalent sphere.

David also gave his deduction for the dynamic factor using Stoke's law and account for both form drag and frictional drag [7]:

$$K = \left[\frac{1}{3}\cdot\frac{d_n}{d_v} + \frac{2}{3}\cdot\frac{d_s}{d_v}\right] \tag{4}$$

Where d_s are the diameter of sphere whose effective surface equals that of the object.

In our research, we build a wind jet using a hair dryer and some masses as the tested object. The trajectory of objects is recorded using a camera and then put on *Tracker* software to track its equilibrium position on top of the jet outlet. Data processing is then carried out to plot graphs and linear regression onto the raw data. Then, we will build a stabilizing set-up using a light, inextensible string to suspend for a non-spherical object inside a jet and then measure the experimental drag using trigonometric deductions. Finally, we will compare the experimental results to the calculated data using the empirical equations mentioned above and comment on the accuracy.

2. Experimental Methods

2.1. Experimental Procedures

2.1.1. Experiment 1

- Select 5 groups of spheres with different masses (2.7 g, 2.9 g, 3.0 g, 3.1 g, 3.3 g), ensuring that the material is uniform and the shape is close to an ideal sphere.
- Adjust the hair dryer to stabilize the airflow and measure the airflow velocity at the nozzle using an anemometer.
- Set up a height measurement system using a camera, taking the bottom of the wind tunnel as the zero reference point. Use the software *Tracker* to record the positions.
- For each group of spheres, repeat the measurement 3 times: release the sphere from the top of the wind tunnel and record the height over time once it reaches stable suspension.
- After completing the recordings, replace the next group of spheres, keeping the wind speed and measurement zero point unchanged, and minimizing environmental interference.

The experimental setup is shown in Fig. 1. At this stage, the drag force is balanced with the weight (i.e., $F_d = W = mg$).

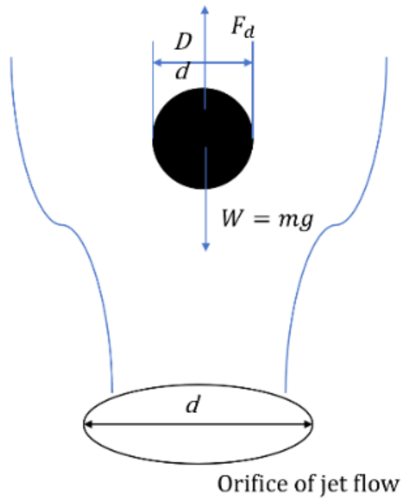

Figure 1. Experimental setup and procedure for Experiment 1

2.1.2. Experiment 2

As shown in Fig. 2, the experiments process can be described as follows:

1. Select a group of non-spherical objects to be measured, including a cuboid, a cylinder, a rectangular prism, and a cylinder with a conical head. Include a sphere for calibration.

2. Adjust the hair dryer to stabilize the airflow and measure the airflow velocity at the nozzle using an anemometer.

3. Set up a height measurement system using a camera, taking the wind tunnel orifice as the zero reference point. Use the software *TRACKER* to record the positions.

4. For each object, repeat the measurement 3 times: release the object from a vertical position and record the horizontal position and the string's angle deviation from its original position while floating in the jet at specified time intervals.

5. After completing the recordings, proceed to the next object, keeping the wind speed and measurement zero point unchanged, while minimizing environmental interference.

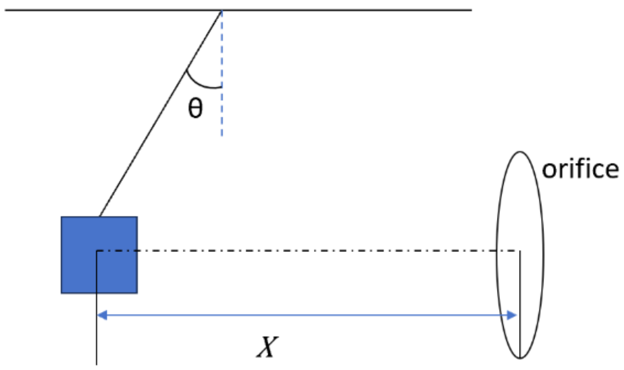

Figure 2. Experimental setup and procedure for Experiment 2

2.2. Introduction and solution of formulas used in the experiment

The core formula of this experiment revolves around the viscous resistance coefficient of the sphere, from which the height can be expressed based on the relative motion between the airflow and the sphere. The formulas and derivation process are as follows:

The drag force is given by:

$$F_d = \frac{1}{2}\rho C_d A v^2 \tag{5}$$

Where ρ is the fluid density, A is the characteristic surface area, C_d is the drag coefficient, and v is the fluid velocity.

For a sphere, the characteristic area is:

$$A = \frac{D^2}{4}\pi \tag{6}$$

Where *D* is the diameter of the sphere.

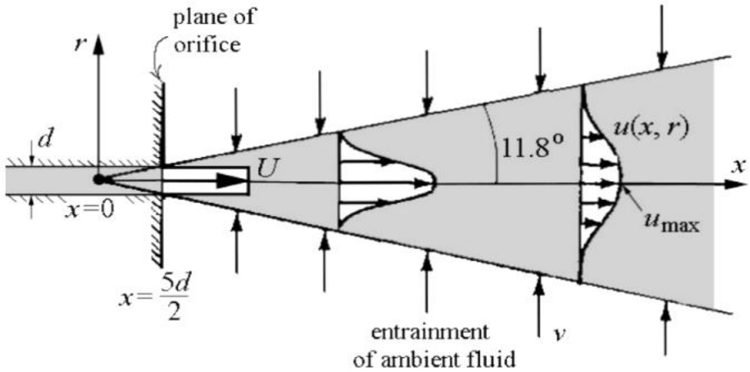

Figure 3. Velocity profile of a jet

As shown in Fig. 3. in a jet from an orifice, the velocity profile varies with the radial distance *r* from the center and the downstream distance *x* from the orifice. Previous investigations by Rajaratnam confirmed that the velocity profile of jets can be expressed as [8]:

$$u(x,r) = U_{max} e^{\left(-\frac{r^2}{2\sigma^2}\right)} \tag{7}$$

Where *x* is the downstream distance along the jet (measured from the virtual source), *r* is the radial distance from the centerline, U_{max} is the centerline velocity, and $\sigma(x)$ is the standard deviation of the velocity distribution.

The maximum velocity is given by:

$$u(x,0) = U_{max} = \frac{5Ud}{x} \tag{8}$$

And the fluid velocity standard deviation is as follows:

$$\sigma = x/10 \tag{9}$$

Combining these, the drag coefficient for a sphere at the center of the jet is:

$$C_d = \frac{8F_d}{\rho u^2 \pi D^2} \tag{10}$$

Vertically, we can replace *x* with *h*:

$$u = \frac{5Ud}{h} \tag{11}$$

$$C_d = \frac{8F_d h^2}{25\rho U^2 d^2 \pi D^2} \tag{12}$$

Thus, the equilibrium height can be expressed as:

$$h = 5UdD\sqrt{\frac{C_d \rho \pi}{8}} \cdot \sqrt{\frac{1}{F_d}} \tag{13}$$

$$F_d = \frac{25 C_d \rho U^2 d^2 \pi D^2}{8h^2} \tag{14}$$

This provides insight into the drag force on a sphere inside a vertical jet. However, non-spherical objects rarely achieve static equilibrium in a vertical jet. Therefore, a light string is used to suspend the object in a horizontal jet, allowing measurement of its position to determine the local fluid velocity.

The drag force is still given by:

$$F_d = \frac{1}{2}\rho C_d A v(x,r)^2 \tag{15}$$

but now the position away from the jet center must be considered, so

$$u(x,r) = U_{max}e^{\left(-\frac{r^2}{2\sigma^2}\right)} \tag{16}$$

From the experimental setup, the relationship between the object's weight and the drag force can be expressed as:

$$\begin{cases} W = T\cos\theta \\ F_d = T\sin\theta \end{cases} \tag{17}$$

$$F_d = \tan\theta\, W \tag{18}$$

and it can also be expressed in terms of fluid viscosity as:

$$F_d = 3\pi\mu d_v \frac{5Ud}{x} K \tag{19}$$

Where θ is the angle of deviation of the string from its original position, W is the weight of the object, and x is the distance from the center of the orifice to the object.

3. Data Processing and Analysis

3.1. Experiment 1

Table 1 shows the data for varying mass and constant jet velocity (1.9ms^{-1}) under sphere conditions.

Table 1. Raw data for sphere at velocity of 1.9m/s

Sphere Mass/g	Equilibrium Height/m	Standard deviation	Weigh/N	$\frac{1}{W}$/N^{-1}	$\sqrt{\frac{1}{W}}$/N$^{-0.5}$
2.7	0.338	0.0421	3.31	0.302	0.549
2.9	0.324	0.0428	3.18	0.314	0.560
3	0.317	0.0225	3.11	0.322	0.567
3.1	0.312	0.0794	3.06	0.327	0.572
3.2	0.31	0.0591	3.04	0.329	0.574

Fig. 4 shows a graph of $\sqrt{\frac{1}{W}}$ against equilibrium height at velocity 1.9m/s.

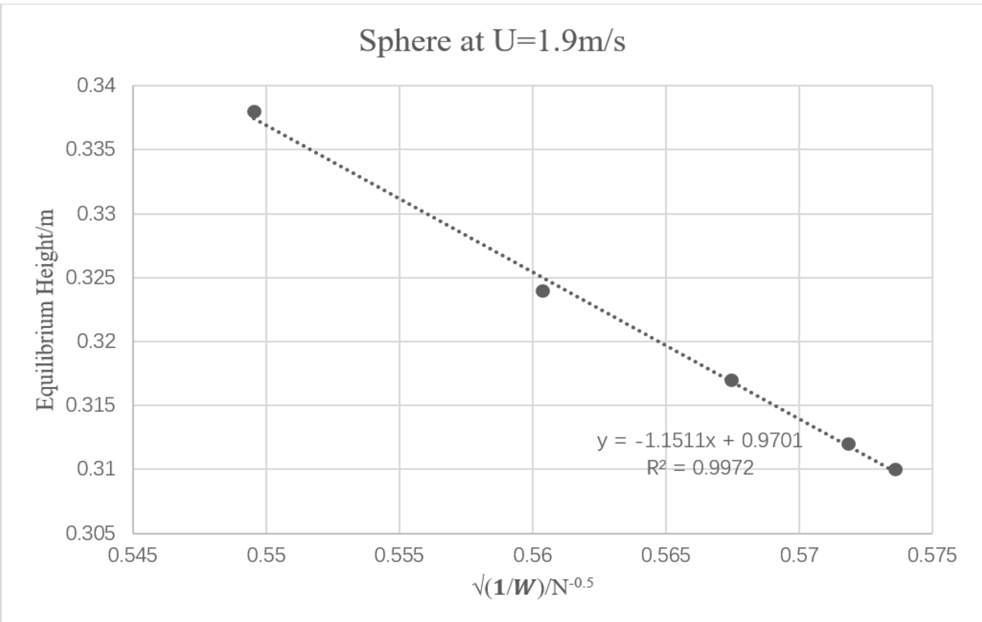

Figure 4. Equilibrium heigh

The average height in the table is the statistical mean of each group of data, reflecting the core position of the stable suspension of the sphere: the smaller the standard deviation (e.g., 0.0225), the smaller the fluctuation of height and the better the repeatability of the experiment. The R^2 value is 0.9972 as shown in the graph, reflecting an accurate linear regression of $\sqrt{\frac{1}{W}}$ to equilibrium height.

3.2. Experiment 2

Table 2 shows the related data for calculation and the actual data measured from the experiment. For this experiment,$u = \frac{5Ud}{x}$,$U = 26.4m/s, x = 30cm, d = 5cm$ Therefore $u = 22m/s$, and $\mu = 1.8 \times 10^{-5} Pa \cdot s$.

Table 2. Raw data for the non-spherical objects

Shape	dv/cm	dn/cm	S/cm2	ds/cm	ψ/cm2	K	K’
cylinder	5.72	5.00	/	2.5	0.873	1.04	0.583
cubid	5.96	5.42	/	2.71	0.806	0.923	0.606
rectangular prism	4.73	4.37	/	1.88	0.789	0.909	0.573
cone head cylinder	6.3	5.00	0.657	2.50	/	0.742	0.529
sphere	/	/	/	/	/	/	/

Table 3. Measured drag force and calculated drag force

Fd/N	Fd’/N	Fdactual/N
0.0221	0.0124	0.0230
0.0205	0.0135	0.0220
0.0161	0.0101	0.0150
0.0174	0.0124	0.0210
0.0143	/	0.0130

For rows 1–3, the drag force Fd is calculated using equation (1), while for row 4 it is determined from equation (2). Both K′and Fd′ are obtained from equation (3). The percentage uncertainty for the sphere is given by

$$\frac{|0.130-0.143|}{0.130} \times 100\% = 10 \tag{20}$$

Therefore, a 10% tolerance is adopted as the experimental uncertainty in subsequent comparisons. The percentage uncertainties corresponding to each method are summarized in Table 4.

Table 4. Uncertainty of different methods

Shape	Method 1 uncertainty	Method 2 uncertainty	Method 3 uncertainty
cylinder	3.90%	/	46.09%
cubid	6.80%	/	61.36%
rectangular prism	7.30%	/	32.67%
cylinder with a cone head	/	17.10%	40.95%

As shown in Table 3, Method 1 yields uncertainties of 3.9%, 6.8%, and 7.3%, respectively. Considering the 10% experimental uncertainty, these values fall within the acceptable range and can therefore be regarded as accurate. The percentage uncertainty tends to increase as the shape changes from a cylinder to a cuboid and then to a rectangular prism. This is likely due to the sharp edges of the prism, which induce boundary turbulence and make it more difficult for numerical calculations to capture accurate values.

Method 2 is applied to calculate the viscous drag of a cylinder with a conical head, producing an uncertainty of 17.10%. Even after accounting for the 10% experimental uncertainty, there remains a residual uncertainty of 7.10%, suggesting that this method may not be sufficiently reliable.

Method 3 results in uncertainties of 46.09%, 61.36%, 32.67%, and 40.95%, which are unacceptably high. This indicates that the method is not convincing for practical use. The large deviations are likely caused by sharp edges or unsmooth surfaces, which lead to turbulence and reduce the accuracy of empirical formulas for viscous drag prediction.

In future work, the experiments could be extended by varying the Reynolds number, since the drag coefficient and consequently the viscous drag, changes with flow conditions [9]. Additionally, further investigation into jet flow at different orientations and with varying dynamic constants would be valuable. Interestingly, analytical solutions for non-spherical objects in incompressible Newtonian media have been reported [10], using the differential transformation method (DTM) to provide deeper theoretical insights. However, such results are often highly complex, whereas approximate empirical approaches are generally sufficient for engineering applications.

4. Conclusion

Overall, Method 1 provides reliable results within the 10% experimental uncertainty and can be considered accurate, particularly for simple geometries such as cylinders. Method 2 shows moderate deviation, making its reliability questionable, while Method 3 produces excessively high uncertainties and is therefore unsuitable. The results suggest that sharp edges and unsmooth surfaces introduce turbulence that reduces the accuracy of empirical formulas for viscous drag estimation. Future work should examine the effect of different Reynolds numbers and flow conditions to improve the applicability of these methods.

Authors Contribution

All the authors contributed equally and their names were listed in alphabetical order.

References

[1] LIST E. Mechanics of turbulent buoyant jets and plumes. HMT: The Science & Applications of Heat and Mass Transfer. Reports, Reviews & Computer Programs, 1982, 1: 1 - 68.

[2] ZHI-GANG F, M E. Drag coefficients of viscous spheres at intermediate and high Reynolds numbers. Journal of Fluids Engineering, 2001, 123 (4): 841 - 849.

[3] HOMANN H, BEC J, GRAUER R. Effect of turbulent fluctuations on the drag and lift forces on a towed sphere. Journal of Fluid Mechanics, 2024, 976: 1 - 25.

[4] FUCHS N A. The mechanics of aerosols. Oxford: Pergamon Press, 1964.

[5] HEISS J F, COULL J. Studies on drag in chemical engineering. Chemical Engineering Progress, 1952, 48 (3): 133 - 140.

[6] BOWEN B D, MASLIYAH J H. Drag on spheres in fluid flow. Canadian Journal of Chemical Engineering, 1973, 51 (1): 8 - 15.

[7] LEITH D. Drag on nonspherical objects. Aerosol Science and Technology, 1987, 6 (2): 153 - 161.

[8] RAJARATNAM N. Turbulent jets. New York: American Elsevier Publishing Company, 1976.

[9] YANG H, FAN M, LIU A, DONG L. General formulas for drag coefficient and settling velocity of spheres based on theoretical law. International Journal of Mining Science and Technology, 2015, 25 (2): 219 - 223.

[10] YAGHOOBI H, TORABI M. Analytical solution for settling of non-spherical particles in incompressible Newtonian media. Powder Technology, 2012, 217: 453 - 463.